Plane Wave Analysis of Panel Wedges

T. Kar and M.L. Munjal[1]

Abstract: In the present work, a wedge structure made of absorbing panels has been analyzed by making use of the matrizant analysis with the help of the Boundary-Condition-Transfer (BCT) algorithm. The rectangular panel wedge, as it is called in this manuscript, is simple in geometry. The theoretical model, based on the plane wave acoustical coupling between multiple interacting ducts of variable cross sectional area, is applied to predict the pressure reflection coefficient of the present wedge configuration. Bulk reaction and hence wave propagation in the wedge material has been assumed in the proposed model. An asymptotic solution using the Peano-Baker series of matrix calculus is derived for different variable area ducts and then solved with the aid of the boundary condition transfer algorithm. A brief parametric study is also included as an aid to designers.

Keyword: Acoustic wedge; plane wave; Matrizant; transfer matrix method; anechoic chamber.

1 Introduction

An anechoic room simulates a free field, a representation of a theoretical infinite space, in which there are no sound wave reflections and hence the wave propagation is free from reverberations. This is achieved by mounting sound absorbing materials on the walls in order to absorb the sound energy. Design of the anechoic chambers is based on the parametric charts developed through an experimental investigation by different investigators [Beranek and Sleeper (1946), Koidan, Hruska, and Pickett (1972)]. Determining the optimum wedge configuration by experimentation is not

cost effective. Thus, an analytical approach for analyzing the acoustic wave propagation in the wedges or panels is imperative. The conventional rectangular wedges were analyzed by means of the finite element method (FEM) and the boundary element method (BEM) to validate the experimental results [Easwaran and Munjal (1993), Wang and Tang (1996)]. They made use of the bulk reaction model that accounts for wave propagation in the wedge material. Incidentally, both of these computational approaches were based on a 2-D analysis.

Like wedges, acoustical panels are also used as sound absorbers, but for different purposes. Conventional wedges are used in the anechoic chambers, whereas panels in different forms find application in various performance spaces like HVAC plenums, blower and compressor enclosures, audiometric test rooms, barrier walls etc. Micro-perforated panels are also used to attenuate relatively low frequency sound wave [Chens, Lee, and Chiang (2000)]. The concept of hybrid panels is based on a combined approach for noise control: a passive approach for middle and higher frequencies and an active approach for low frequencies. Such acoustic absorbers have been studied experimentally in the literature [Lee, Kim, Rhee, Jo, and Choi (2002)].

In terms of the cut-off frequency, the threshold frequency above which the pressure reflection coefficient is less than 0.1 for a plane wave at normal incidence, and the sound absorption coefficient of an acoustic wedge is less than 0.01, there is a significant difference between the performances of a simple panel and the rectangular wedge. Wedges have very low cut-off frequencies, whereas the acoustic panels provide good sound absorption only at higher frequencies. Here, an attempt is made to get a rectangular wedge structure from

[1] Facility for Research in Technical Acoustics, Department of Mechanical Engineering, IISc, Bangalore -560 012, India. Corresponding author: Tel.: +91 80 22932303; Fax: +91 80 23600648 Email: munjal@mecheng.iisc.ernet.in

the flat panels that would offer an intermediate performance. The schematic diagram of such a configuration is given in Fig. 1.
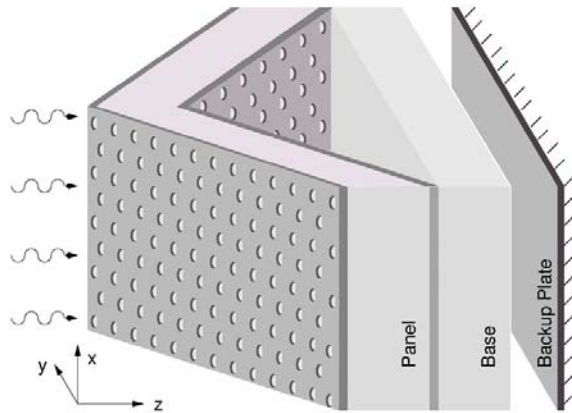

Figure 1: Schematic diagram of the panel wedge.

Structurally non-rigid wedges need to be protected by a perforated metal sheet and/or a thin impervious membrane. HVAC applications may make use of fibrous absorbers with a perforated plate as the protective layer. Apart from imparting the structural stability, perforated plate is used to protect the fibrous absorbing material. An experimental investigation shows that the physical elements of such a sound absorptive system like porosity, thickness of the facing, the density of the porous backing material etc. can change the specific acoustic impedance of the absorber and hence its absorption coefficient [Davern (1977)]. The rectangular wedges have been analyzed in the literature to determine the pressure reflection coefficient where the predicted results were validated with their experimental, BE and FE counterparts [Kar and Munjal (2006a)].

The semi-analytical approach, proposed here, makes use of the plane wave propagation and a wave coupling between the wedge and the surrounding air cavity. The model considers the porous absorptive material as an equivalent fluid with complex dynamic density ρ_ω and sound speed c_ω [Wang (1999)]. With the above analytical assumption, the sound wave seems to interact between a couple of fluid sub domains. The resulting differential equations are solved by means of the matrizant analysis with the aid of

the boundary condition transfer (BCT) algorithm [Kar and Munjal (2005)]. The model presented here, applies to any configuration as long as there exists a finite value of interface impedance. Although the present model addresses fibrous materials with a perforated metal facing, yet it can also accommodate the alternate applications of the unwrapped panel wedges with the assumption of a "*pseudo-coupling coefficient*", a small fictitious impedance at the interface, for the sake of generalization [Kar and Munjal (2006a)]. The concept of *pseudo-coupling coefficient* is a mathematical need of the approach adopted here.

2   Mathematical model for wave propagation

As shown in Fig. 1, the present model consists of three distinct structural zones. The first is the tapered panel. This zone is made of a couple of parallel perforated plates packed with fibrous sound absorbing material between them. It may be noted that the panel is mirror symmetric with respect to the x-z plane. A base made of an open-pore foam backs this. The base is structurally stable and needs no perforated plate backing. In case the base is designed to be made of similar fibrous material like that of the panel, it must be protected by perforated plate in a similar manner. Dissimilar sound absorbing materials for the panel and the base bring forth the concept of a hybrid panel wedge. This may make the overall wedge effective over a wide frequency range. Thickness of the air gap between the panel and the base varies linearly with respect to the y-axis. The final part is an air gap that terminates at a rigid backup plate.

The mathematical model, presented in this section, deals with determination of the transfer matrices for each of the constituent domains. Fig. 2 shows the mathematical domains of the wedge. The complete wedge comprises five distinct parts (computational domains). Each of them will be treated independently during the analysis. As shown in Fig. 2, the tapered panel of length L consists of three distinct computational domains. They are denoted as $\Xi_1, \Xi_2,$ and $\Xi_3,$ respectively. Due to the parallelogram-like cross-sectional area of the panel, lengths of the segments Ξ_1 and Ξ_3 are equal $(L_1 = L_3)$. The segment Ξ_4 represents the

base of Length L_4, whereas the final segment Ξ_5 of length L_5 is basically an air gap at the back of the wedge. Each segment is modeled as a perforated element with multiple interacting ducts [Kar and Munjal (2006b)] of variable cross-sectional area [Kar and Munjal (2004)]. In the present analysis, each section/computational domain is assumed to be made up of ducts, i.e., the domain Ξ_2 is a three-duct configuration. The mathematical model accounts for a cross flow across the perforated plate, [Munjal (1987)]. The assumption of bulk reaction and hence wave propagation in the absorptive material holds good in the present analysis. Determination of the transfer matrix across the panel of the wedge (domains Ξ_1, Ξ_2, and Ξ_3) is the primal part of the analysis.
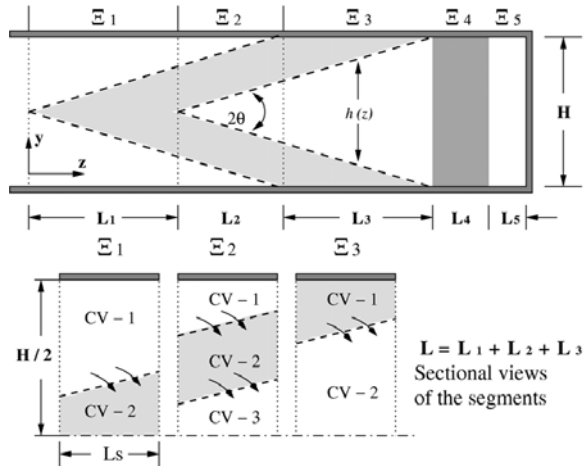

Figure 2: (A): Schematic diagram of the two-segment conical concentric tube resonator. (B): The corresponding simple concentric tube resonators.

Due to the finite perforate impedance, the pressure difference across the interface of the wedge and the air cavity drives a vibrating acoustic mass across their interface. The above vibrating mass appears in the continuity equations of both the sub-domains in terms of the transverse velocity, which leads to an acoustic wave coupling between the sub-domains in terms of pressures. The perforate impedance at the interface causes the acoustic coupling between the ducts for any individual segment of the panel. Due to its geometrical symmetry with respect to the x-z plane, it would

be sufficient to analyze half of the structure for plane wave propagation in the wedge. The wedge may be assumed to be placed inside an impedance tube with a square cross-section of overall transverse dimension "H''". The segments Ξ_1 and Ξ_3 are treated as two interacting variable-area rectangular ducts, whereas the segment Ξ_2 is a three-duct configuration. The base (Ξ_4) and the air gap (Ξ_5) at the back are considered as uniform area ducts.

Assumptions that simplify the mathematical formulation of the governing equations are as follows:

- Spatial variations of acoustic pressure and thence density, across the wave fronts in any domain are negligible in the frequency range of interest here.

- Amplitudes of pressure and density perturbations in ducts are negligible compared to their mean values.

- Temperature variation and viscous effect of the medium are negligible.

- Perforation along the entire length of the tube is uniform.

- Wall thickness of the perforated shield is negligible as compared to the transverse dimension of the panel of the wedge.

- The porous absorbent material of any duct is considered as an equivalent fluid with complex wave number k_ω, complex density ρ_ω, and characteristic impedance Y_ω.

3 Mass continuity

The generalized model, presented here, is applicable to all the sections. Here, the model will be illustrated over the section Ξ_1. The wave propagating medium in the panel is either air or the sound absorbing material.

Let ρ_0 be the time-mean component of the air density, and $\rho_1(z,t)$ and $u_1(z,t)$ be the density and the particle velocity perturbations over the cross-sectional area $S_1(z)$, respectively. Similarly $\rho_2(z,t)$ and $u_2(z,t)$ are the density and velocity perturbations for the second control volume and

are averaged over the area $S_2(z)$. Then, the linearized form of the continuity equation for the control volume 1 may be written as

$$\frac{\partial \rho_1}{\partial t} + \rho_0 u_1' + u_1 \rho_0 (\ln S_1)' + \frac{2H u_{12}^* \rho_0}{S_1 \cos \theta} = 0, \quad (1)$$

and the corresponding continuity equation for the second duct (CV-2) is given by

$$\frac{\partial \rho_2}{\partial t} + \rho_\omega u_2' + u_2 \rho_\omega (\ln S_2)' - \frac{2H u_{12}^* \rho_\omega}{S_2 \cos \theta} = 0, \quad (2)$$

where u_{12}^* is the normal particle velocity at the interface, and assumed to be positive for the normally inward direction (from CV-1 to CV-2). A prime ($'$) denotes differentiation with respect to z.

4 Momentum conservation

The momentum equations of the cavities for dynamical equilibrium become

$$\rho_0 \left[\frac{\partial u_1}{\partial t} \right] + p_1' = 0; \text{ and } \rho_\omega \left[\frac{\partial u_2}{\partial t} \right] + p_2' = 0, \quad (3)$$

The fluctuating normal particle velocity u_{12}^* across the perforate in Eqs. 1 and 2 is due to the pressure difference at the interface and may be given as

$$u_{12}^* = \frac{p_1(z) - p_2(z)}{\rho_0 c_0 \zeta}, \quad (4)$$

where c_0 is the sound speed in air and ζ is the non-dimensional perforated impedance for a perforated plate of thickness t_h, hole diameter d_h, and porosity σ, and may be given as [Selamet, Lee, Ji and Huff (2001)]:

$$\zeta = \frac{6 \times 10^{-3} + j k_0 \left(t_h + 0.375 \left(1 + \frac{k_w Y_w}{k_0 Y_0} \right) d_h \right)}{\sigma} \quad (5)$$

The complex valued density ρ_ω of Eq. 2 is determined from the corresponding wave number k_ω and characteristic impedance of the absorptive material Y_ω. For any such sound absorbing material, Y_ω and k_ω are precisely outlined by empirical

formulae of Delany and Bazley (1970), later improved through modifications by Mechel (1976):

$$\frac{Y_\omega}{Y_0} = \begin{cases} 1 + 0.0485 \, (A)^{0.754} - j 0.087 \, (A)^{0.73}; \\ \qquad\qquad\qquad \text{if } A \leq 60 \\ \frac{0.5(A/\pi)j1.4}{(-1.466 + j0.212A)^{0.5}}; \\ \qquad\qquad\qquad \text{if } A > 60 \end{cases}$$

$$\frac{k_\omega}{k_0} = \begin{cases} 1 + 0.0978 \, (A)^{0.6929} - j 0.189 \, (A)^{0.6185}; \\ \qquad\qquad\qquad \text{if } A \leq 60 \\ (-1.466 + j0.212A)^{0.5}; \\ \qquad\qquad\qquad \text{if } A > 60 \end{cases}$$

$$(6)$$

where Y_0 and k_0 are the characteristic impedance ($\rho_0 c_0$) and the wave number (ω/c_0) of air, respectively. The normalized flow resistivity "A" of a λ-deep acoustic lining, is given by $A = \eta \lambda / Y_0$, where η is the flow resistivity of the lining material. Impedance expressions for different arbitrary bodies are available in the literature [Chandrasekhar and Rao (2006), Han and Atluri (2006)].

Similarly, the equations for domains Ξ_2 and Ξ_3 may be framed accordingly. For the section Ξ_2, the variable depth air gap between the panel and the base constitute the third duct. Eventually, there exist a particle velocity at the interface of the control volumes CV-2 and CV-3 as well. The control volume CV-2 of Ξ_2 has a uniform cross-sectional area.

5 Solution

The pressure reflection coefficient of the panel wedge is derived from its transfer matrix, a matrix that transfers the state vector along the z coordinate, making use of the following steps [Kar and Munjal (2006a)].

- The system matrix $[\mho_i]$ for each domain Ξ_i, $i = 1$-5, is derived from the respective differential coefficients.

- Forward transfer matrices $[\mho_i]$ from the corresponding system matrices $[\mho_i]$ are deter-

mined by making use of the matrizant analysis.

- The four-pole transfer matrix $[T]$ is determined by applying the boundary conditions over the transfer matrices $[\mathbf{\Omega}_i]$. Here, the boundary condition transfer (BCT) algorithm is made use of to overcome the computational instabilities as discussed in the earlier literature [Kar and Munjal (2005)].

- The pressure reflection coefficient and hence the sound absorption coefficient is derived from the transfer matrix $[T]$.

The first two steps are similar for all the domains with little difference between them. Thus, here, only one domain, namely $[\mathbf{\Xi}_i]$, will be worked out. The third step applies the boundary conditions of any domain to its forward transfer matrices $[\mathbf{\Omega}]$. The final step is independent of the sub domains and is applied to the four-pole matrix derived over the whole wedge structure.

For plane wave propagation in fluids, state variables like the acoustic pressure p_i, density perturbation ρ_i and velocity perturbations u_i over the corresponding areas $S_i(z)$ are all harmonic functions of time. Working in the frequency domain, the time dependence of all variables may be taken as harmonic ($e^{j\omega t}$). For steady state simple harmonic motion,

$$\left.\begin{array}{l} p_i(z,t) = p_i(z)e^{j\omega t} \\ u_i(z,t) = u_i(z)e^{j\omega t} \\ u_{12}^*(z,t) = u_{12}^*(z)e^{j\omega t} \end{array}\right\} i = 1,2. \tag{7}$$

Using the condition of isentropicity, the density and the pressure perturbations are related by [Munjal (1987)]

$$p_i = \rho_i c_i^2; \quad i = 1,2 \tag{8}$$

Using Eq. 8, the density terms, ρ_1 and ρ_2, are eliminated from the continuity equations in favor of the corresponding acoustic pressures. Expressing transverse velocity as in Eq. 4, the set of four governing equations Eqs. 1-3 can be given as a set of four coupled differential equations with variable coefficients. The derivative of each state variable may be rearranged as a linear combination of the state variables (acoustic pressure and particle velocity). Thus,

$$\frac{d\{V\}_i}{dz} = \sum_{k=1}^{4} [\Psi]_{ik}\{V\}_k; \quad i = 1 \text{ to } 4, \text{ or} \tag{9}$$
$$\{V'\} = [\Psi]\{V\}$$

where the state vector $\{\mathbf{V}\}$ may be written as

$$\{V\} = \begin{cases} \begin{bmatrix} p_1 & u_1 & p_2 & u_2 \end{bmatrix} \\ \qquad\qquad \text{for domains } \Xi_1 \text{ and } \Xi_3 \\ \begin{bmatrix} p_1 & u_1 & p_2 & u_2 & p_3 & u_3 \end{bmatrix} \\ \qquad\qquad \text{for domain } \Xi_2 \end{cases} \tag{10}$$

Here, it may be reported again that only the solution for the segment $\mathbf{\Xi}_1$ is presented in this section. To clarify Eq. 9, one of the vector component, say $\{V\}_2$, corresponding to the particle velocity u_1, can be derived by rearranging Eq. 1 and is given below explicitly.

$$u_1' \equiv \frac{d\{V\}_2}{dz} = -\left\{\frac{ik_0}{Y_0} + \frac{2H}{S_1\cos\theta Y_0\zeta}\right\}p_1 +$$
$$\left\{\frac{2H}{S_1\cos\theta Y_0\zeta}\right\}p_2 - (\ln S_1)' u_1. \tag{11}$$

Terms associated with the vector components p_1, p_2, etc. are elements of the system matrix $[\mho]$. Order of the system matrix is dependent upon the number of space variables associated with the corresponding section. $[\mho]_1$ and $[\mho]_3$, corresponding to the sections $\mathbf{\Xi}_1$ and $\mathbf{\Xi}_3$, respectively, are fourth order square matrices, whereas, for $\mathbf{\Xi}_2$, the number of differential equations will be six and thus the corresponding system matrix $[\mho]_2$ is of the sixth order. An asymptotic method of matrix integration, better known as Peano-Baker method, may be used for solving the set of Eqs. 9, where the forward transfer matrix $[\Omega]$ is determined from the corresponding system matrices $[\mho]$ in the form of an infinite series [Frazer, Duncan and Collar (1952)]. This approach does not decouple the set of first order differential equations and hence no change undergoes in their order. Here, the solution in terms of the transfer

matrix $[\Omega]$ for the corresponding section may be given as:

$$\{V\}_{z=0} = [\Omega]\{V\}_{z=L}, \tag{12}$$

where

$$[\Omega] = [I_n + Q[\mho] + Q[\mho]Q[\mho] + \cdots]^{-1}$$

$$Q[\mho] = \int_0^L [\mho]\,dz$$

$$Q[\mho]Q[\mho] = \int_0^L [\mho]\left(\int_0^L [\mho]\,dz\right)dz \tag{13}$$

Its usefulness is limited by slow convergence since the solution starts from the identity matrix on every occasion. The constituent matrix elements $[\mho]_{ik}$ of Eq. 9 are either constants or some continuous functions of the axial co-ordinate z. Thus, there exists a definite integral for each of them and thence an approximated solution for the first order differential equation of Eq. 9 over any continuous path $z = z_1$ to $z = z_2$. This functional continuity attribute of the coefficients provides an alternate solution. Systems with variable coefficients can be solved by splitting the entire range of the independent variable z into a finite number of sub-segments. The variable coefficients may be integrated over each of the sub-domain and this would provide an averaged out system matrix with constant coefficients. An element of the corresponding system matrix in this case is given as:

$$\left[\int_{z_1}^{z_2} [\mho]\,dz\right]_{ik} = \int_{z_1}^{z_2} [\mho]_{ik}\,dz, \tag{14}$$

where $(z_1, z_2) \subset (0, L_i)$. The constituent elements of a matrix, that result from the integration of the matrix $[\mho]$ over the path (z_1, z_2), correspond to the average value of the integral $[\mho]_{ik}$ over that interval. Thus, a scalar valued matrix (where $[\mho]_{ik} =$ constant, for all i, k) may be integrated over the entire path as a single segment. But for the variable $[\mho]_{ik}$'s, the interval $\{z_1 < z < L_1\}$ needs to be segmented for better approximation. Let this interval (path of integration) be divided into a finite

number of equal segments (say $\mathbf{N}$). Thus, the integration for a single segment may be worked out over the path length of $L_s (= L_1/\mathbf{N})$. Error associated with the approximation depends upon the number of segments as well as the characteristics of the functions $[\mho]_{ik}$. Thus, for any such interval that spans $(z, z + L_s)$, the state vectors at the boundaries are related as [Kar and Munjal (2004)]

$$\{V\}_z = e^{[\Gamma]}\{V\}_{z+L_s}; \quad [\Gamma]_{ik} = -\int_z^{z+L_s} [\mho]_{ik}\,dz, \tag{15}$$

The Maclaurin's series may be used to expand the transfer matrix $e^{[\Gamma]}$ that acts as a linear operator (matrix multiplication) between the downstream and upstream state vectors of one segment.

$$e^{[\Gamma]} = [I_N] + \sum_{n=1}^{\infty} \frac{[\Gamma]^n}{n!} \equiv [\Phi], \quad \text{(say)} \tag{16}$$

If the transfer matrix $[\Gamma]$ is diagonalized using the corresponding modal matrix $[\Psi]$ and the eigenvalues of the matrix $[\Gamma]$, then

$$[\Gamma] = [\Psi][\lambda][\Psi]^{-1}, [\Phi] = [\Psi]\left[e^{\lambda}\right][\Psi]^{-1}, \tag{17}$$

where eigenvalues are elements of the diagonalized matrix $[\lambda]$:

$$\left[e^{\lambda}\right]_{ik} = \begin{cases} e^{\lambda_i} & \text{if } i = k \\ 0 & \text{if } i \neq k \end{cases} \tag{18}$$

and $[\lambda]_i$ is the ith eigenvalue. Care must be taken to ensure the direction of the integration while integrating the matrix $[\mho]$. The process is repeated for all segments, and the corresponding transfer matrices are determined and sequentially multiplied to produce the overall transfer matrix:

$$[\Omega] = \left[\prod_{i=1}^{\mathbf{N}} [\Phi]_i\right]. \tag{19}$$

Similarly, the transfer matrices for other sections Ξ_2 to Ξ_5 of Fig. 2 are derived. The orders of the matrices are different. Eqs. 9 are a two-point boundary value problem; that is, it is required to satisfy boundary conditions at more than one

value of the independent variable. The preference for the proposed semi-analytical method over the standard numerical methods is twofold. The foremost need is to get an operator in terms of the transfer matrix that operates between the vectors at the two ends of the conical part of wedge. Due to large difference between the impedances offered by different domains, it seems to have produced numerical instability generated due to the cross flow of the sound propagation while satisfying the boundary conditions across the independent variable. Here, the transmission of the boundary condition along the independent variable is basically a numerical cancellation of the associated differential coefficients ($[\mho]_{ik}$ of Eq. 9).

6 Boundary Condition

The order of the overall transfer matrices $[\Omega_i]$ varies from domain to domain; the order of the linear operator for Ξ_1 and Ξ_3 is four, whereas it is six for Ξ_2. Suitable boundary conditions are applied to obtain the desired four-pole parameter transfer matrix $[T]$. The highest dimension of any state vector of Eq. 10 is six (vectors across the domain Ξ_2). Thus, the desired four-pole parameter transfer matrix $[T]_1$, relating the state vectors across the panel (domains Ξ_1, Ξ_2, and Ξ_3), may be obtained by applying a set of four appropriate boundary conditions (B.C.) to the transmission matrices $[\Omega_i]$, $i = 1$ to 3.

Before obtaining a single transfer matrix over the sections Ξ_1, Ξ_2, and Ξ_3, two of the boundary conditions are applied to section Ξ_2. The normal particle velocity at the outlet of the first duct and at the inlet of the third duct of Ξ_2 may be considered to be zero. They may be given as

$$u_{1,(z=L_1+L_2)} = u_{3,(z=L_1)} = 0. \tag{20}$$

On applying the boundary conditions of Eq. 19, the order of the transfer matrix $[\Omega_2]$ is reduced by two. The reduced transfer matrix $[\Omega_2]$ of order four may now operate between the vectors with four elements each across Ξ_2. It may be written

as

$$\begin{bmatrix} p_1 & u_1 & p_2 & u_2 \end{bmatrix}^T_{(z=L_1)}$$
$$= [\Omega_2] \begin{bmatrix} p_2 & u_2 & p_3 & u_3 \end{bmatrix}^T_{(z=L_1+L_2)}. \tag{21}$$

Now, all three transfer matrices $[\Omega_1]$, $[\Omega_2]$ and $[\Omega_3]$, which are of the same order, are multiplied sequentially. To reduce the above product matrix into the desired 2x2 matrix, a couple of boundary conditions are applied. The normal particle velocity at the inlet ($z = 0$) of the second duct of Ξ_1 may be considered to be zero. Similarly, the velocity at the outlet ($z = L$) of the first duct of Ξ_3 is zero. Thus, the boundary conditions may be written as

$$u_{2,(z=0)}\big|_{\Xi_1} = u_{2,(z=L)}\big|_{\Xi_3} = 0. \tag{22}$$

As followed in all existing literature, matrix $[\Omega]$, with the help of elementary algebra, may be reduced to a four-pole matrix $[T]_1$ by applying the B.C.'s of Eq. 21. The base segment Ξ_4, packed with absorptive material, and the air gap Ξ_5 of Fig. 2 are treated as ducts with uniform cross-sectional areas. The respective transfer matrices $[T]_2$ and $[T]_3$ may be given as [Munjal (1987)],

$$[T]_2 = \begin{bmatrix} \cos(k_\omega L_4) & j\frac{\sin(k_\omega L_4)}{Y_\omega} \\ jY_\omega \sin(k_\omega L_4) & \cos(k_\omega L_4) \end{bmatrix};$$

$$[T]_3 = \begin{bmatrix} \cos(k_0 L_5) & j\frac{\sin(k_0 L_5)}{Y_0} \\ jY_0 \sin(k_0 L_5) & \cos(k_0 L_5) \end{bmatrix}, \tag{23}$$

The final transfer matrix relating the state vector at the extreme ends is obtained by sequential multiplication of the three constituent segmental transfer matrices. Thus,

$$[T] = \prod_{i=1}^{3} [T]_i \text{ and } \begin{bmatrix} p & u \end{bmatrix}^T_{z=0} = [T] \begin{bmatrix} p & u \end{bmatrix}^T_{z=L}. \tag{24}$$

The impedance Z and thus the pressure reflection coefficient R at the incident plane may be evaluated from the transfer matrix $[T]$. Assuming a rigid termination (the particle velocity $u = 0$) at the end of the air-gap (domain Ξ_5), the acoustic impedance Z and the reflection coefficient R may be given as

$$Z = \frac{T_{1,1}}{T_{2,1}} \text{ and } R = \frac{Z - Y_0}{Z + Y_0}, \quad Y_0 = \rho_0 c_0 \tag{25}$$

In the present work, the expression for ζ is evaluated from the default option values of $t_h = 1$ mm, $d_h = 3$ mm and $\sigma = 0.3$ (porosity of 30 %). In case, the panel is not protected by the perforated plate (a case of pressure continuity at the interface) or the impedance at the interface is too small, the elements of the transfer matrices $[\Omega_i]$ become large. Application of B.C.'s to a matrix may be viewed as a set of algebraic operations involving the constituent elements of the matrix. Thus, any algebraic computation involving astronomically large numbers would generate computational instabilities on an expected line. In such situations, the conventional approach of applying B.C.'s would be inefficient for predicting the impedance Z and the reflection coefficient R of an acoustic wedge. The BCT algorithm is known to overcome such limitations [Kar and Munjal (2005 and 2006a)].

7 Application of BCT algorithm

Boundary conditions are applied over a matrix to reduce the order of the matrix by means of a sequence of arithmetic operations. Every computing machine has its own accuracy limit; say of the order of 10^{-16} or 10^{-24}. So, the accuracy of the application of the boundary conditions depends upon the numerical values of the transfer matrix elements/components. The magnitudes of the transfer matrix elements depend upon the impedance at the interface and the axial dimension of the acoustic domain [Kar and Munjal (2006a)]. Details of the algorithm are left out from the scope of the current manuscript and may be referred to in the literature [Kar and Munjal (2005)]. Yet, a brief description will be outlined here. In the present method, each boundary condition is represented as a relationship among the vector elements (particle velocity and the acoustic pressure), where any one component of an nth order vector may be given in terms of a linear combination of the rest of the components. Such relationship, an algebraic function by itself, for a unique vector may be given as:

$$\{V\}_k = f(\{V\}_i \,|\, \forall i = 1 \text{ to } n, i \neq k) \qquad (26)$$

where $\{V\}_k$ is the kth component of the vector $\{V\}$. The above may be demonstrated for a domain over the length L, where second order square matrices $[A]$ and $[B]$ operate over the spans $(0, L/2)$ and $(L/2, L)$, respectively, so that

$$\{u\} = [A]\{v\} \text{ and } \{u\} = [B]\{w\} \qquad (27)$$

where

$$\{u\} = [u_1 \; u_2]^T; \; \{v\} = [v_1 \; v_2]^T \text{ and }$$
$$\{w\} = [w_1 \; w_2]^T. \qquad (28)$$

As mentioned earlier, the boundary condition applied on the vector $\{u\}$ may be represented as

$$u_2 = C_1 u_1 + C_0 \qquad (29)$$

where the coefficients C_0 and C_1 are known quantities, i.e., for acoustic domains, coefficients are given in terms of impedance or admittance. A similar relationship for the vector $\{v\}$ may be developed by making use of the matrix $[A]$:

$$v_2 = D_1 v_1 + D_0 \qquad (30)$$

where

$$D_0 = \frac{C_0}{A_{22} - C_1 A_{12}}; \quad D_1 = \frac{C_1 A_{11} - A_{21}}{A_{22} - C_1 A_{12}}. \qquad (31)$$

The set of coefficients (D_0, D_1) can be hypothetically considered as a boundary condition applied to the vector $\{v\}$. Rather than applying the given boundary condition (in terms of C_0 and C_1) on the vector $\{u\}$ over a single overall matrix $([M]=[A][B])$, where the matrix elements are larger than those of the individual matrices, it is numerically advantageous to apply different set of coefficients over segmental matrices $[A]$ and $[B]$. This is the essence of the BCT algorithm.

8 Results and Discussion

The present approach has been applied to the simple rectangular wedge structures in the literature [Kar and Munjal (2006a)] and is corroborated with its experimental [Koidan, Hruska and Pickett (1972)], FEM [Easwaran and Munjal (1993)] and BEM [Wang and Tang (1996)] counterparts. Here, the panel wedge has been analyzed to show the utility of the present semi-analytical approach based on the plane wave theory. All numerical

computations were performed for sonic speed of 340 m/s. The transverse dimensions "H" and the panel length L ($L = L_1 + L_2 + L_3$) have the default option values of 0.3 m and 0.44 m respectively, whereas L_1 and L_3 are 0.14 m long each. Unless mentioned otherwise, the flow resistivity of the acoustic materials in panel (η) as well as the base (η_b) has the default value of 1.6×10^4 Ns/m^4. The base length L_4 and air gap length L_5 are taken constant at 0.1 m each.

Fig. 3 shows the pressure reflection coefficients (R) for different values of the flow resistivity of the panel. The pressure reflection coefficient for different values of flow resistivity differs substantially at the lower frequencies when it increases with increasing value of η. This is due to the higher resistance offered by the fibrous material to absorb sound energy. Beyond a certain value of η, the performance deteriorates on further increments. Here, the sound wave experiences a higher impedance mismatch at the interface and thus fails to enter the panel. This leads to a stronger reflection back to the source. So, there is a limiting value of flow resistivity for an optimal sound absorption coefficient.
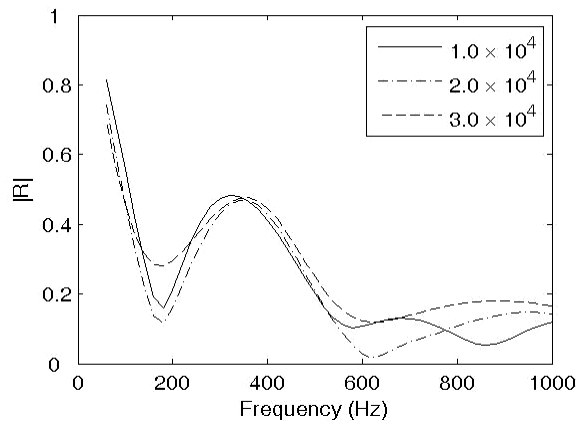
Figure 3: Pressure reflection coefficient for different values of the flow resistivity of the panel (η).– – –, 1.0×10^4; – · –, 2.0×10^4 and ——, 3.0×10^4 Ns/m^4.

For a constant overall panel length L, and $L_1 = L_3$, the shape of the panel changes with length L_1. Effect of L_1 on pressure reflection coefficient is shown in Fig. 4. A set of four curves has been
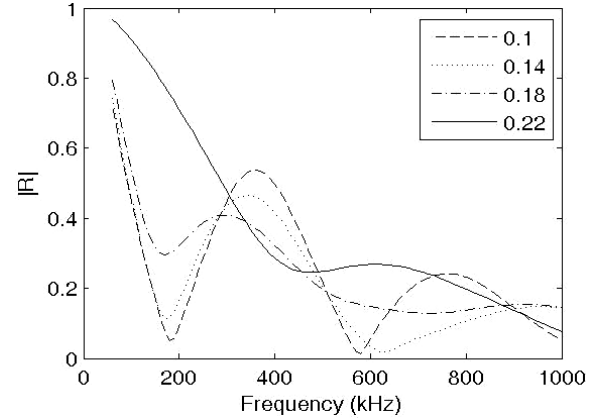
Figure 4: Pressure reflection coefficient for different values of L_1 for $\eta = \eta_b$ =1.6×10^4 Ns/m^4 and $L = 0.44$ m. – – –, 0.1 m; · · · · · ·, 0.15 m; – · – , 0.18 m and ——, 0.22 m.

shown. They exhibit a common trend. While comparing any two of them, it may be noticed that whichever has got a lower trough, has got a higher peak. This is due to the following reasons. For a smaller value of length L_1 (with $L = L_1 + L_2 + L_3$ fixed), the included angle θ of Fig. 2 of the domain Ξ_2 is less, and so is also the depth (perpendicular distance between both the perforated plates) of the panel. Thus, a panel with smaller L_1 would offer lower impedance and hence a lower pressure reflection coefficient. Performance of the panel wedge at the next frequency band (200-400 Hz) is controlled by the air-cavity between the panel and the base. The smaller the value of L_1, the larger the cavity volume. This cavity acts as a compliance of a resonator and controls the amplitude of the reflection coefficient.

Fig. 5 shows the pressure reflection coefficient for different values of the panel length L. Longer panels have lower pressure reflection coefficient. But with a constant L_1, the trapped air cavity at the back of the panel becomes larger for longer elements. As mentioned above, this large volume resonator raises the peak of the reflection coefficient spectrum. So, there is an optimal value of the panel length for which the absorption coefficient will be the most desirable.
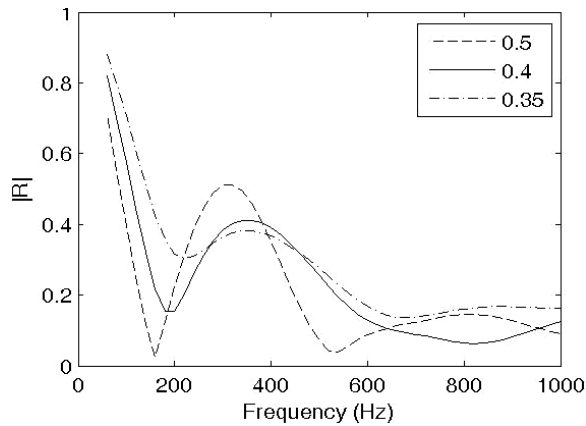
Figure 5: Pressure reflection coefficient for different values of L for $\eta = \eta_b$ =1.6×10^4 Ns/m^4 and L_1 = 0.15 m. – – –, 0.5 m; ——, 0.4 m and – · –, 0.35 m.

9   Concluding Remarks

Here, an alternative to both the conventional wedge and the flat panel has been analyzed. The *"panel wedge"*, as it has been termed here, has an intermediate performance level. The panel is analyzed by making use of the matrix calculus and the boundary condition transfer algorithm. A parametric study has been performed for some of the geometrical attributes of the panel wedge. Unlike the conventional wedge, the air cavity has its distinct signature over the pressure reflection coefficient.

References

Beranek, L. L.; Sleeper, H. P. (1946): The design and construction of anechoic sound chambers. *J Acoust Soc Am,* vol. 18, pp. 140-150.

Chandrasekhar, B.; Sadasiva M. Rao. (2006): Acoustic Scattering from Fluid Bodies of Arbitrary Shape. *CMES* vol. 21(1), pp. 67-80.

Chens, W. -H.; Lee, F. -C.; Chiang, D. -M. (2000): On the acoustic absorption of porous materials with different surface shapes and perfo-

rated plates. *J Sound Vib,* vol. 237(2), pp. 337-355.

Davern, W. A. (1977): Perforated facings backed with porous materials as sound absorbers - an experimental study. *Applied Acoust,* vol. 10(2), pp. 85-112.

Delany, M. E.; Bazley, B. N. (1970): Acoustical characteristics of fibrous absorbent material. *Applied Acoust,* vol. 3(2), pp. 106-116.

Easwaran, V.; Munjal, M. L. (1993): Finite element analysis of wedges used in anechoic chambers. *J Sound Vib*, vol. 160(2), pp. 333-350.

Frazer, R. A.; Duncan, W. J.; Collar, A. R. (1952): *Elementary matrices and Some Applications to Dynamics and Differential Equations*, Cambridge University Press.

Han, Z. D.; Atluri, S. N. (2006): A Systematic Approach for the Development of Weakly-Singular BIEs, *CMES,* vol. 21(1), pp. 41-52.

Kar, T.; Munjal, M. L. (2004): Analysis and design of conical concentric tube resonators. *J Acoust Soc Am,* vol. 116(1), pp. 74-83.

Kar, T.; Munjal, M. L. (2005): An inherently stable boundary-condition-transfer algorithm for muffler analysis. *J Acoust Soc Am,* vol. 118(1), pp. 60-71.

Kar, T.; Munjal, M. L. (2006a): Plane Wave analysis of acoustic wedges using the Boundary-Condition-Transfer algorithm. *Applied Acoust,* vol. 67(9), pp. 901-917.

Kar, T.; Munjal, M. L. (2006b): Analysis of multiple-duct variable area perforated tube resonators. *International J Acoust Vibration,* vol. 11(1), pp. 19-26.

Koidan, W.; Hruska, G. R.; Pickett, M. A. (1972): Wedge design for National Bureau of Standards anechoic chamber. *J Acoust Soc Am,* vol. 52(4), pp. 1071-1076.

Lee, J. -K.; Kim, J.; Rhee, C. J.; Jo, C. -H.; Choi, S. -B. (2002): Noise reduction of passive and active hybrid panels. *Smart Mater. Struct.* vol. 11(6), pp. 940-946.

Mechel, F. P. (1976): Extension to low frequencies of the formulae of Delany and Bazley for absorbing materials. *Acustica*, vol. 35, pp. 210-213

(in German).

Munjal, M. L. (1987): Acoustics of Ducts and Mufflers. John Wiley, New York.

Selamet, A.; Lee, I. J.; Ji, Z. L.; Huff, N. T. (2001): Acoustic attenuation performance of perforated absorbing silencers. *SAE Noise and Vibration Conference Paper*, 2001-01-1435.

Wang, C. N.; Tang, M. K. (1996): Boundary element evaluation on the performance of sound absorbing wedges for anechoic chambers. *Engg. Analysis with Boundary Elements*, vol. 18(2), pp. 103-110.

Wang, C. N. (1999): Numerical decoupling analysis of a resonator with absorbent material. *Applied Acoust*, vol. 58(2), pp. 109-122.